Enhanced thermal efficiency organic Rankine cycle for renewable power generation

U. Caldiño Herrera [a], J.C. García [b], F.Z. Sierra-Espinosa [b,*], J.A. Rodríguez [b], O.A. Jaramillo [c], O. De Santiago [d], S. Tilvaldiev [a]

[a] Universidad Autónoma de Ciudad Juárez, Av. Plutarco Elías Calles 1210, Ciudad Juárez, Chihuahua 32310, Mexico
[b] Universidad Autónoma del Estado de Morelos, Av. Universidad 1001, UAEM, Cuernavaca, Morelos 62209, Mexico
[c] Instituto de Energías Renovables, Universidad Nacional Autónoma de México, Priv. Xochicalco s/n, Temixco, Morelos 62580, Mexico
[d] ETU i+D, Cuauhtémoc 3, Ind. San Pedrito Peñuelas, Querétaro 76148, Mexico

ARTICLE INFO

ABSTRACT

The Organic Rankine Cycle (ORC) technology is recognized to supply electricity from low temperature waste heat and solar energy sources. When the ORC system is heated by solar energy it uses two-fluids and two-loops, producing a relatively low thermal efficiency. To increase the ORC applicability, a solar energy assisted ORC system of single loop is proposed. The aim is to reduce the ORC heat transfer losses, minimize the equipment initial and maintenance cost and enhance the thermal efficiency. This is achieved by using bladder tanks which may improve drastically the ORC technical and economic performance. This method allows the heating to vary in the collector keeping the turbine inlet condition as a constant, impacting on the heat transfer losses and simplifying the configuration. The paper shows that an ORC of a single fluid can keep a constant turbine inlet despite the mass flow rate variations due to the suńs radiation incidence, therefore, reducing the risk of likely faults in the turbine caused by high frequency vibration. An ORC enhanced 10.54% thermal efficiency is obtained with 0.5 kg/s of R1233zd(E) and a pressure ratio = 5, powered by parabolic trough collectors to generate 10 kW during eight hours per day. The ORC competitiveness is dictated by a total generation cost of 54.3 $/MWh and the advantages of a single working-fluid single loop simplicity for overall configuration.

1. Introduction

Global demand for energy consumption increases despite the variable prices of fossil fuel and its negative effects on the environment. The consequence is that the ratio of using conventional energy sources to alternative technologies for a variety of applications is continuously reducing [1]. Low-grade heat sources like solar, geothermal, biomass, surface seawater, and waste heat are thus clean and sustainable alternatives [2–6], suitable as for driving an organic Rankine cycle (ORC) with multipurpose applications [7,8]. Focusing on the generation of electricity, examples of installed plants worldwide use this technology, which also demonstrate their cost-effective potential [3,6,7,9]. Achievement of these goals means that several constraints must be overcome: the expander to drive the electrical generator, typically a turbine, directly affects the efficiency of the system given that its designed for the working fluid properties, energy source temperature, flow rate, condensing pressure and goal power output [10]. Also, the

best operating condition for the highest turbine efficiency demands a high speed [5,6,10]. This situation leads to unsuitability for the direct coupling to a grid synchronous running speed [11]. Regarding the working fluid, it must be specifically selected according to the source of heating, the site climate conditions and load conditions [5,6,12–16]. For instance, R245fa is used with flat plate solar collectors in a layout of rolling piston expander to obtain 1.73 kW and thermal efficiency of 3.2% [17]. With evacuated solar collectors the system reaches an isentropic expander efficiency of 45.2% and a thermal efficiency of 4.2%. Instead, with a regenerator the thermal efficiency goes to 3.67% [18], which may still improve if the mass flow of the working fluid could offset the influence from unsteady solar radiation. Another solution for increasing the applicability of the ORC technology is the use of thermal energy storage (TES), because it allows the ORC to operate with low solar radiation, or even running using a different R123 working fluid, and powering with parabolic trough or flat plate solar collectors [19,20]. The TES approach basically allows to overcome the variable nature of solar radiation using heat storage materials to interact through

---

* Corresponding author.
E-mail address: fse@uaem.mx (F.Z. Sierra-Espinosa).

Nomenclature

A	PTC Area, m^2
C_{total}	total specific cost rate, \$/kWh, \$/MWh
MO	operating cost, %
$m, \dot{m}$	mass flow rate, kg/s
n	operation years
OH	the operating hours per year
oh	superheating temperature of working fluid
P	power, W
P_R	pressure ratio
P_1, P_2, P_3, P_4	pressure through the Organic Rankine Cycle thermodynamic stages, Pa
$\dot{Q}$	available radiation heat flux
q'	heat flux per unit area
$\dot{q}$	specific heat per unit of mass,
s	specific entropy, kJ/kg K
t	time, min
T	temperature, K
V	volume, m^3
X, k_1, k_2, k_3	constants for each equipment in the ORC
Z_i	operation cost, \$
$Z_{i_{sp}}$	specific operation cost, \$/kW
z	fixed interest rate, %

Greek letters

Δ	Difference
ρ	density, kg/m^3
η	efficiency
ω	specific work, kJ/kg

Subscripts

Col	solar collector
e	time for which the mass of fluid starts entering the turbine
evap	evaporator, evaporation
fluid	working fluid
i	equipment of the ORC
inc	solar radiation incidence surface
min	minimum
max	maximum
net	net
0	time at which the pump stops pumping mass of fluid to the collector
PST	pressure storage tank
p, pump	pump
s	isentropic
sat	saturation
TST	thermal storage tank
th	thermal
t, turb	turbine
rad	radiation

sensible heat transfer with the working fluid [21–26]. However, it involves the use of two fluids instead of only one, implicating more steps of heat transfer in detriment of the efficiency. For instance, Delgado-Torres et al. [21,22] analyzed and optimized a solar assisted ORC reverse osmosis desalination system using different working fluids as butane, isobutane, R245ca and R245fa and four configurations of solar collectors. Calise et al. [23] studied a 6-kW solar power plant operating with evacuated flat solar collectors, using a diathermic oil storage tank to mitigate any variations of thermal conditions due to fluctuations of radiation along the day. A constant thermal yearly efficiency of 10% with a solar collector's efficiency from 50% in summer to 20% in winter resulted given the variations of Mediterranean climates. In general, the irradiance variation during the day, and from one place to another seems one of the main concerns. Freeman et al. [24] analyzed 2 different types of solar collectors: a high-performance evacuated flat-plate and an evacuated-tube heat-pipe, for two different locations: London, and Laranca, Cyprus. The TES approach allowed to keep a small temperature difference of 5 degree in the source heat exchanger to obtain an 80-kW power output, assuming fixed isentropic efficiency for both, the pump, and the expander [25,26]. Quoilin et al. [27] combined parabolic trough collector and thermal storage unit packed bed of quartzite for a remote power generation solar ORC. Combined domestic heating/cooling can be achieved with solar energy in bio-climatic building architectures, but not driven by ORC systems [28–30]. Alternatively, TES schemes with latent heat transfer involves phase change materials, PCM, like paraffins, water, stearic acid and n-octadecane but the melting point of materials limits the applications to temperatures between 273 and 333 K, or like Erythritol and RT100 for higher limits to 353 and 493 K [30]. However, the performance of the system is affected by the poor thermal conductivity of the PCM material [30,31], despite recent efforts tried to reduce this drawback [32,33]. Other example of TES for higher melting temperatures above 573 K is the concentrating solar plants that use PCMs like salt (NaCl) [31]. In summary, combined ORC/thermal energy storage relies on a second working fluid or a material for latent or sensible heat transfer in a second loop, suitable for high temperature applications, far from the objectives of the ORC proposed in this work.

Besides, the literature survey indicates that the ORC performance parameters are maximized for unique configuration and specific conditions. In this sense, one goal in this work is a low-cost ORC scheme regarding other experiences [34]. The system is proposed for electricity generation of small-scale to support affordable and sustainable solutions to several applications, including the residential lighting. The simplicity of this ORC relies on only one loop with a single working fluid despite the effects of any mass flow rate variation in the solar collector derived from variable solar radiation incidence. A second goal consists of controlling a constant flow rate that feeds the turbine. The method is to allow the mass flow rate variation in the collection field to maintain a constant storage temperature, giving place to held constant the mass flow rate and fluid properties at the turbine inlet throughout the day. Therefore, the low-cost goal includes the operation design as well as the layout of this ORC. The turbine is the most valuable element of the cycle. As failure reports show, the damage of operating turbines exposed to frequent flow rate fluctuations include low and high frequency vibration ending in engine failures in a short time of operation, reducing drastically the useful life of the turbine [35–37]. Turbines respond to mass flow rate variations in several ways. Long term vibration can be due to erosion caused by cavitation of the suction side of the blades, or abrasion of the pressure blade side. Fatigue of leading-suction edges or bearings results in units subject to mass flow variable conditions [35]. Therefore, the present design considers keeping the mass flow rate in the turbine as a constant because turbines are considered the main element of an ORC system, given their influence on the overall efficiency, and their cost, especially looking for reduced operating and maintenance costs, avoiding the low/high frequency vibrations from pressure variations. To achieve this goal the scheme considers a bladder tank placed after the solar collection outlet and prior to the turbinés fluid inlet. A bladder tank allows the volume variations without affecting the pressure because it has inside a flexible polymeric membrane [38,39]. Therefore, the working fluid accumulates in the storage tank as a superheated vapor without any phase change or use of PCM. The fluid is then released at a constant mass flow rate to ensure a continuous and constant speed in the turbine, independently of how the working fluid fluctuates in the solar

collecting field as a response to solar energy changes along the day. The way this ORC system stores sensible thermal energy makes use of an elastomer that keeps the working fluid without variation of pressure and temperature, neither phase-change, which allows to regulate the mass flow rate that feds the turbine. Although the use of bladder tanks involves thermal storage, there is not any phase-change material, therefore, the present design is out of the traditional scheme of thermal storage system, TES.

The novelty and originality of the paper and highlighting the main contributions may be stated as: A solar driven ORC system is proposed considering the solar radiation along an 8-h operation. The solar radiation is not constant during the operation time; thereby, to achieve the same thermodynamic conditions at the solar collector outlet, a varying mass flow rate is needed. The value of mass flow rate depends entirely on the instantaneous available solar radiation so a control valve working with the solar radiation information is used for this purpose. Regarding the varying mass flow rate required in the solar collector, the turbine needs a constant mass flow rate to operate safely with the maximum efficiency. Therefore, a novel configuration is proposed to achieve these operating conditions: a bladder tank is used in between the solar collector outlet and the turbine inlet. This storage tank must ensure the availability of the working fluid to feed the turbine inlet regarding the solar collector mass flow rate. It also must keep the thermodynamic properties without any change.

To test the ORC design proposed in this work, a set parabolic trough solar energy collector (PTC) of recent development [40], is connected for a demand of 10 kW. The test is set to the conditions of solar radiation at Temixco, Morelos, a small city located 18.86-degree North latitude and −99.23 longitude and situated at 1299 m above sea level, in the central region of Mexico. The results indicate a fluid R245fa as the most suitable working fluid to obtain a thermal efficiency $n_{th} = 10.11\%$. It is shown that low volume storage is required, which includes two tanks, one of 66.82 m³ and another of 2.11 m³ for the superheated vapor and saturated liquid, respectively. The global cost of electricity generation using different technologies is analyzed. A comparison of present ORC with concentrating solar energy shows a total specific cost on the order of $ 0.0543/kWh, which represents an ORC plant output of a high level of competitiveness.

2. Methodology

2.1. System configuration

The ORC configuration is shown in Fig. 1a and 1b. A cycle of four thermodynamic states, one for each component: pump, evaporator, turbine, and condenser, constitutes the simplest ORC [19,22,24]. Starting in the pump: the fluid pressure increases from saturated liquid state condition (1), 300 K, to the evaporating pressure. A control valve located after the pump is used for the mass flow rate in the solar collector. This control valve regulates the flow by a control system in which the input parameter is the solar radiation. Using this information and the turbine inlet temperature design condition, the mass flow rate is calculated.

In the evaporator, state 2, the solar collector transfers heat from solar radiation to the working fluid in an isobaric process, until reaching a final condition of 5 K superheated vapor, state 3. The broken line in Fig. 1b indicates phase change. Overheating temperature is defined to avoid any possible pressure drop in the evaporating process due to irreversibility. This condition also prevents that humid vapor reaches the turbine's inlet since pressure drop still ensures superheated vapor, state 4. In this stage, heat transfer from the collection to the working fluid considers energy losses which depend on the temperature difference between the collection surface and the working fluid and radiation of heat [34]. Since the energy input varies during the operating time, the collection efficiency varies as well. Thus, to maintain the same thermodynamic conditions at the outlet evaporator regardless of any energy input variation, the mass flow rate must vary as a function of daytime. This mass flow rate turns out to be the turbine storage tank (TST) inlet. For the TST outlet, a constant mass flow rate is required. To ensure this condition, the tank must operate with a constant pressure, which is achieved with a bladder tank, which is explained below.

The literature presents a variety of expander designs for similar ORC systems to the proposed. These include axial and radial turbine expanders, and piston positive displacement, as well as scroll and screw volume expanders [8,41]. Many of the parameters to consider like the mass flow rate, the pressure ratio, the temperature level, and the speed of rotation combined with the properties of the working fluid are defined by the size of the ORC system. In this work a radial income turbine expander was designed based on the efficiency diagram [42,43]. The turbine incorporates a geometry of blade designed by third order Bezier
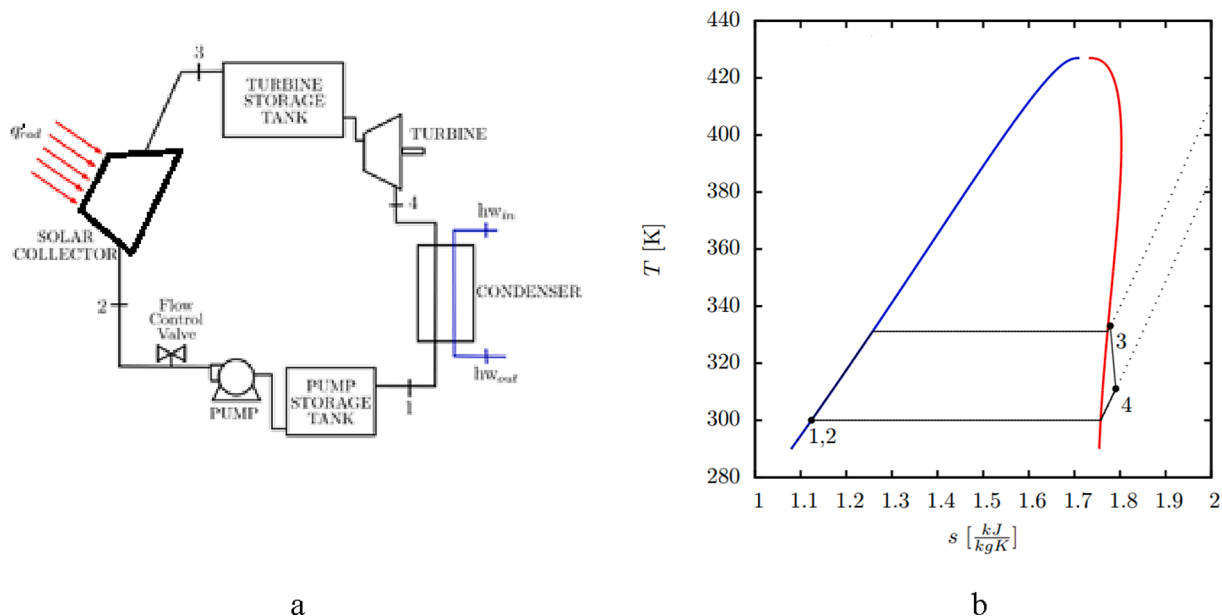

a

b

Fig. 1. Layout of the ORC system; a) Elements of the thermodynamic cycle; b) T-s diagram for R245fa as a working fluid.

curves and high performance for 10 kW power output [44–51]. Fig. 2 shows both, an isometric and the plan views of the radial income turbine. Blades in this design are camber line optimized to reduce the risk of misalignment with the flow from the inlet to outlet. The turbine characteristics are listed in Fig. 2c. For a further detailed description, the reader is referred elsewhere [47].

A storage tank (TST) between the evaporator and the turbine, after state 3 has the advantage that there is no need for a secondary loop in the PTC, which could increase the loss of heat transfer to the working fluid. The TST compensates the variable mass flow rate from the evaporator while supplying a constant mass flow rate to the turbine, which is the desired operating condition.

Because TST stores a variable amount of fluid with a bladder tank, given its capacity to keep the fluid at constant pressure regardless of the volume variation. For this purpose, it is important to ensure that working fluid enters the TST, which depends on the bladder tank pressure. The pressure condition is set to a slightly smaller value than the evaporating pressure. A bladder tank serves to control pressure variations in the cycle pipeline created by solar energy transient behavior [38,52]. Piping systems including a bladder tank can meet standard codes like B31.3 and B31.4 sections by ASME, which apply for this kind or piping system [52].

It is through flexible materials that the bladder tank cumulates energy timely and releases the stored energy as pressure relief a time delay. The bladder tank is used to store energy in two ways: the first one is thermally, because the working fluid enters the tank in a superheated state at high temperature from the PTC array. The vapor remains in this condition since the tank is a heat insulation due low conductivity polypropylene that deforms to get the whole volume after peak radiation hours. The second way of storing energy is pressuring, because the flexible material absorbs energy keeping the superheated vapor at high pressure. The study considers a calculation of the thermal efficiency by coupling the turbine to the solar collector (evaporator) through the bladder tank, and daily averaged value of turbine, pump power and thermal energy in the collector.

The ORC operation requires availability of working fluid for turbine's feeding, which is satisfied whenever the average inlet mass flow rate equals the outlet mass flow rate. Also, for the starting stage of operation, the TST mass balance equation must include only the inlet condition. Once in the turbine, the working fluid expands until it reaches the condensation pressure at entropy change because of work produced, state 4. For that, isentropic efficiency is assumed, which is set to 0.8 [47–51].

In the condenser the working fluid changes phase from superheated vapor to saturated liquid, states 4 and 1, after which a second tank, the pressure storage tank (PST) is used to feed the pump with the variable mass flow rate required in the collection stage. This PST a has constant mass flow rate as inlet and a variable mass flow rate as output. PST is a second bladder tank, which ensures constant pressure regardless of any variation of volume.

2.2. Working fluid

A selection of fluids from the CoolProp library [53] was conducted based on the saturation conditions for condensation pressure and temperature for the site of operation. The pump inlet condition is assumed as saturated liquid pressure at 300 K. In the condenser a temperature difference of 5 degree between the working fluid and the cooling fluid is stated. Any organic fluid having saturation pressure between 1 and 1.6 bar and temperature at 300 K may be a candidate for working fluid. Condensation takes place at ambient temperature and pressure but never at vacuum conditions/below atmospheric pressure. Four candidates for working fluid meet these conditions as shown in Table 1 [53]. The maximum temperature in the PTC is always below 110 °C, and the maximum temperature for every working fluid under consideration for a pressure rate PR = 6 are shown in Table 1. Although R11 has a high ODP and has been phased out, this study considers it to conduct a comparative ORC performance with acceptable fluids, which can be thermodynamically classified by GWP.

2.3. Thermodynamic model

Cubic equations of state were used to calculate the thermodynamic and transport properties for working fluids following Jacobsen et al. [57], which require two known properties for the same state. State 1 in Fig. 1a is calculated for pump inlet temperature of 300 K, saturated conditions and zero vapor quality. State 2 corresponds to the pump outlet, where the pressure increases from P_1 to P_2 as:

$$P_2 = P_1 P_R \tag{1}$$

where P_R is the pressure ratio, which defines the thermodynamic behavior of the ORC. In considering an ideal final enthalpy of the process, an isentropic efficiency for the pump demands the actual enthalpy for state 2, h_2, using the following expression:

$$h_2 = h_1 + \frac{(h_{2s} - h_1)}{\eta_{pumpp}} \tag{2}$$

State 2 is also the condition of inlet to the collector. The heat transfer process that occurs in this device is isobaric, so $P_3 = P_2$. Whichever the irradiation available is, the solar collector outlet temperature T_3 is fixed to be 5 K above the saturation line, which on time is a function of the evaporating pressure for each working fluid. T_3 increases as pressure increases with vapor quality of 1, as:
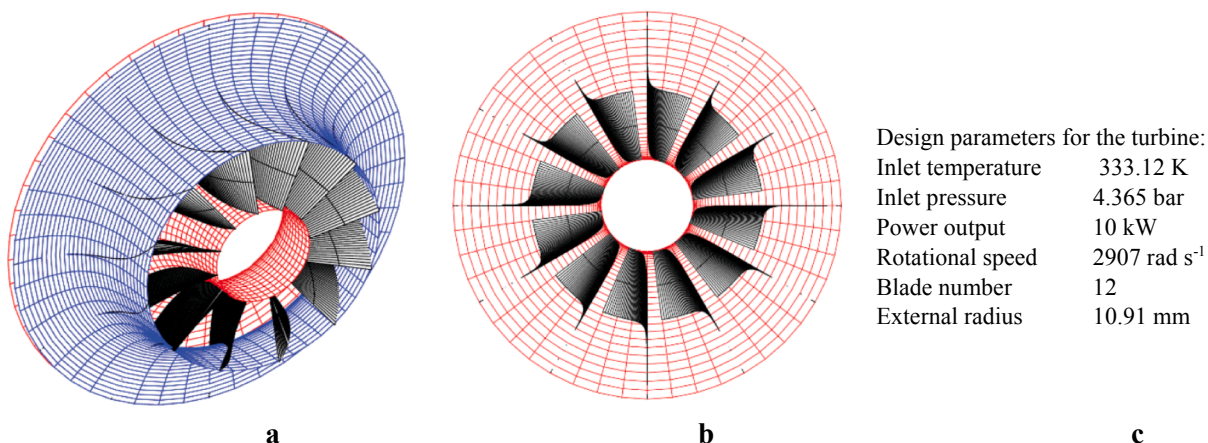

Design parameters for the turbine:

Inlet temperature	333.12 K
Inlet pressure	4.365 bar
Power output	10 kW
Rotational speed	2907 rad s^{-1}
Blade number	12
External radius	10.91 mm

a **b** **c**

Fig. 2. Radial inflow turbine; a) Isometric of shrouded blade rotor; b) Plan view of the unshrouded rotor; c) Main characteristics of turbine design.

Table 1
Saturation pressure at 300 K, and maximum operating conditions for each candidate working fluid [53].

Fluid	Saturation pressure (bar)	ODP	GWP classification	Operating pressure (Pa)	Operating temperature (°C)	Thermal stability (°C)
R11	1.131	1	4600	636279.1	98.33	150 [54]
R245fa	1.590	0	950	891486.4	94.95	250 [54]
R1233zd(E)	1.386	0.00034	1	2990690.1	109.41	175 [55]
R245ca	1.076	0	610	601819.6	92.02	250 [54,56]

$$T_3 = T_{3sat} + Oh \tag{3}$$

where Oh represents the superheating degree of working fluid at the turbine's inlet. Once knowing T_3 and P_3, it is possible to calculate the enthalpy and density (same as collector outlet).

To complete the ORC, the condition for state 4, at the turbine's outlet and condenser's inlet is calculated as follows. The condensing process is assumed as isobaric, $P_4 = P_1$, therefore, an isentropic expansion in the turbine results on an ideal enthalpy h_{4s}. Using this ideal enthalpy and the turbine's isentropic efficiency η_{turb} the actual enthalpy at the turbine's outlet is computed using the following equation:

$$h_4 = h_3 - \eta_{turb}(h_3 - h_{4s}) \tag{4}$$

Thus, the ORC is defined as a thermodynamic cycle. However, the mass flow rate at the evaporator must be controlled to ensure proper operation with any available energy input. Therefore, an average mass flow rate in the evaporator must equal a constant mass flow rate in the turbine. First, the available radiation heat flux, $\dot{Q}_{evap}$ is calculated using Equation (5):

$$\dot{Q}_{evap} = \eta_{col}q'_{rad}A_{inc} \tag{5}$$

where η_{col} is the efficiency of the collector, q'_{rad} is the heat flux per unit area and A_{inc} represents the surface needed to collect any solar radiation incidence. A_{inc} is the surface area for collecting the radiative incidence q'_{rad}, which is known from measured data; an efficiency of collecting, η_{col} depends on the collector configuration, based on a temperature difference between the working fluid and the ambient condition as:

$$\eta_{col} = \frac{\Delta T_{col}}{q'_{rad}} \tag{6}$$

On the other hand, the heat flux received in the collector $\dot{Q}_{col}$ is a function of the initial and final thermodynamic states of the mass flow $\dot{m}$ that circulates through it as:

$$\dot{Q}_{col} = \dot{m}_{col}(h_3 - h_2) \tag{7}$$

By equating Equations (5) and (7), a mass flow rate can be calculated to reach the ORC thermodynamic conditions:

$$\dot{m}_{col} = \frac{\eta_{col}q'_{rad}A_{inc}}{(h_3 - h_2)} \tag{8}$$

However, the solar radiation magnitude changes instantaneously making the data along the daily operating time be defined by a sub-index i in Equation (8), thus Equation (8) swaps to Equation (9) as:

$$\dot{m}_{coli} = \frac{\eta_{col}q'_{rad}A_{inc}}{(h_3 - h_2)} \tag{9}$$

As this parameter varies along the day, η_{col} also does.

A total mass of working fluid results for all solar radiation data during the day, which is measured in a solar station at an elapsed time of 10 min, where 10-min increments for a 9-h operation gives 54 steps. The fluid flow starts every day at 8:00 h circulating in the collector hence storing in TST with no turbine feeding. It is at 9:00 h when the exit valve for TST superheated vapor opens to run the turbine, which stops at 17:00 h when the electricity generation process ends.

Thus, the total mass is:

$$m_{fluid} = \frac{1}{54}\sum_{i}^{54}\dot{m}_{coli}\cdot 600 \text{ s} \tag{10}$$

Therefore, a mass flow rate during the 9-h period is defined as:

$$\dot{m}_{fluid} = \frac{m_{fluid}}{32400 \text{ s}} \tag{11}$$

In the same way, the total mass during a working day divided by the time when the ORC is going to generate electricity, defines the mass flow rate of income to the turbine, which is set by the power output $\dot{W}_{turb}$ for the thermodynamic conditions of the ORC system as:

$$\dot{m}_{turb} = \frac{\dot{W}_{turb}}{h_3 - h_4} \tag{12}$$

An iterative process leads to satisfy the condition of flow rate, where the convergence indicates that the collecting surface A_{inc} fits the ORC thermodynamic conditions. To achieve this, the collecting surface A_{inc} must fit the average value of the mass flow rate in the collector and the mass flow rate in the turbine as:

$$\dot{m}_{fluid} = \dot{m}_{turb} \tag{13}$$

Thereby, an initial value of A_{inc} is proposed, subsequently it increases if:

$$\dot{m}_{fluid} < \dot{m}_{turb} \tag{14}$$

Otherwise A_{inc} reduces if:

$$\dot{m}_{fluid} > \dot{m}_{turb} \tag{15}$$

Therefore, a convergence criterion is set to the maximum difference allowed amongst both flows, and the iterative process to define the value of A_{inc} stops when this criterion is satisfied:

$$\dot{m}_{fluid} \neq \dot{m}_{turb} \leq 0.0001 \text{ kg/s} \tag{16}$$

Once the collecting surface A_{inc} is defined, the performance parameters are calculated as follows. The calculation starts with the specific work in both, the turbine, ω_{turb} and the pump, ω_{pump}, where kinetic energy is neglected, as:

$$\omega_{turb} = h_3 - h_4 \tag{17}$$

$$\omega_{pump} = h_2 - h_1 \tag{18}$$

where a net work is calculated as $\omega_{net} = \omega_{turb} - \omega_{pump}$. The heat supplied to the evaporator is given in Equation (5), thus the specific heat per unit of mass reads as:

$$\dot{q}_{evap} = \frac{\eta_{col}q'_{rad}A_{inc}}{\dot{m}_{col}} \tag{19}$$

Finally, the thermal efficiency η_{th} is calculated as the ratio between the solar radiation collected and the net work developed in the ORC system, the mechanical power in the turbine less the work spent in the pump. Since the input energy is varying along with the daily operation, an average value for daily operation is defined as:

$$\eta_{th} = \frac{(\omega_{turb} - \omega_{pump})}{\dot{q}_{evap}} \tag{20}$$

2.4. Bladder tanks size calculation

The capacity of the tanks TST and PST is calculated in this section. The calculation for saturated liquid PST starts by applying a mass balance for the initial condition of the ORC operation, for the condition of no-running turbine. This tank must contain the total mass of working fluid used during the daytime for the ORC operation. This is understood given that at the end of the day no fluid remains in the TST, while the total mass rests in the PST for starting a new working day. This means that there is no working fluid in the TST while the working fluid mass in the PST is maximum. Applying the mass conservation *principle*, from Equation (10) we have an expression for the PST volume as:

$$V_{PST}(t) = \frac{m_{fluid}}{\rho_1} \tag{21}$$

The mass of fluid m_{fluid} is pumped to the collection field at a variable rate. A time t_e after the fluid starts to circulate through the collector it enters the TST. Only after a time t_e the fluid in the TST already in the condition of superheated vapor starts to enter the turbine at a constant rate. The amount of fluid, sufficient to ensure that the turbine runs without any variations and without stopping, is a function of such a time t_e, which is defined by a mass balance in both tanks, the PST and the TST. Starting the volume calculation with the mass of fluid required in the TST:

$$m_{TST}(t) = \int_t^{t_e} \dot{m}(t) \cdot t dt \ \text{ for } \ t < t_e \tag{22}$$

where:

t, is the instantaneous time for which the calculation of mass fluid in the TST is conducted.
t_e, is the time for which the mass of fluid starts entering the turbine.

After the time t_e we have another condition given by the mass of fluid in the TST:

$$m_{TST}(t) = m_{TST}(t_e) + \int_{t_e}^{t_0} \dot{m}(t) \cdot (t - t_e) dt - \int_{t_e}^{t_0} \dot{m}_{fluid} \cdot (t - t_e) dt \ \text{ for } \ t_e < t < t_0 \tag{23}$$

where:

t_0, is the time at which the pump stops pumping mass of fluid to the collector, say after 9 h of operating the ORC each day. After the time t_0 the mass balance in the TST reads:

$$m_{TST}(t) = m_{TST}(t_0) - \int_{t_0}^t \dot{m}_{fluid} \cdot (t - t_0) dt \ \text{ for } \ t > t_0 \tag{24}$$

Which represents the outflow of the remaining fluid in the TST after the pump is turned off.

Similarly, the PST volume calculation starts with the mass of fluid in the TST during the first minutes of operation of the system, when no fluid is going through the turbine giving a mass of fluid balance:

$$m_{PST}(t) = m_{PST}(t_0) - \int_t^{t_e} \dot{m}(t) \cdot t dt \ \text{ for } \ t < t_e \tag{25}$$

After the time t_e we have another condition given by the mass of fluid in the PST:

$$m_{PST}(t) = m_{PST}(t_e) - \int_{t_e}^{t_0} \dot{m}(t) \cdot (t - t_e) dt + \int_{t_e}^{t_0} \dot{m}_{fluid} \cdot (t - t_e) dt \ \text{ for } \ t_e < t < t_0 \tag{26}$$

After the time t_0, after the pump is turned off and the remining fluid

in the TST is passed through the turbine, the mass balance in the PST reads:

$$m_{PST}(t) = m_{PST}(t_0) + \int_{t_0}^t \dot{m}_{fluid} \cdot (t - t_0) dt \ \text{ for } \ t > t_0 \tag{27}$$

where the same sub-indexes for Equations (22)–(24) apply. For calculating the volume of PST an initial value of $m_{PST}(t_0)$ is proposed. This value changes according to any variation of fluid mass in the tank to avoid negative values. This process leads to minimizing the total volume of PST ensuring the mass fluid availability for the ORC operation. As the mass flow rate in the evaporator $\dot{m}_i$ is not a continuous function of time, a numerical calculation is conducted with a time step of 10 min, see Equation (10). Instead, a fixed mass flow rate is needed at the turbine inlet. This condition requires the TST to store fluid during the starting stage of ORC on a basis of daily operation. A period $t_e = 50 min$ with a lock outlet flow is allowed before opening the outlet of TST. The time of 50 min was selected through an iteration process, in which the mass of fluid in both, the PST and the TST tanks was calculated for different times t_e and paying special attention to the minimum value of mass in both tanks. Mathematically it is possible to get a negative mass of fluid in the tanks which physically has no meaning. Thereby, the time $t_e = 50 min$ allows the availability of working fluid in TST. The reason is to ensure a continuous operation for the ORC system, avoiding any lack of fluid at any time of ORC work.

Since the TST is designed to store the working fluid in the condition of superheated vapor regarding any variation in the evaporator mass flow rate, it requires constant thermodynamic conditions in the TST. The volume of fluid in this tank is calculated as the largest volume required for the operation of the ORC system shown in Equations (28) and (29):

$$V_{TST}(t) = \frac{m_{TST}(t)}{\rho_3} \tag{28}$$

$$V_{TST} = \max[V_{TST}(t)] \tag{29}$$

On the other hand, the PST stores the working fluid as a saturated liquid. Its volume is given by Equation (30). The volume of the tank corresponds to the maximum volume stored during the operation of the ORC and this value depends directly on the initial volume of the PST. To minimize the volume of the tank, the minimum volume of fluid stored during the operation of the ORC is set to zero. To do this, the initial mass contained in the PST is set to be the maximum mass stored in the TST because of the mass conservation principle. By making this calculation, the volume of the PST is defined as:

$$V_{PST}(t) = \frac{m_{PST}(t)}{\rho_1} \tag{30}$$

$$V_{PST} = V_{TST} \frac{\rho_1}{\rho_3} \tag{31}$$

2.5. Techno-economic analysis

This section presents the ORC system as an economic solution for a specific application. A total investment required by the ORC system is based on purchased equipment costs (PEC_i), which is calculated as follows [58]:

$$log_{10} PEC_i = k_1 + k_2 \cdot log_{10} X + k_3 \cdot (log_{10} X)^2 \tag{32}$$

where X, k_1, k_2, k_3 are constants for each element considered in the layout of Fig. 1 a. Values for constants of Equation (32) are provided in Table 2 [58–59]. We assume the use of a peristaltic pump, of size calculated for the mass flow rate 0.5 kg/s and a pressure ratio $P_R = 5$. The condenser is considered a U pass single pipe. For turbines, it is the cost of commercial units as discussed below, as well as the cost of PTC/m^2, to make it comparable with other proposals. Saturated tanks were

Table 2
Constants for PEC_i calculation, Equation (32) [58,59].

i Equipment	Units	X	k_1	k_2	k_3
1 pump	(kW)	1.05	3.5793	0.3208	0.0285
2 condenser	(m^2)	400	3.2138	0.2688	0.07961
3 turbine	(kW)	10	3.1143	0.6923	0
4 PTC	(m^2)	341.11	5.0775	0.699	0
5 TST	(m^3)	66.87	3.9484	0.712	0.1717
6 PST	(m^3)	2.11	3.4746	0.5893	0.2053

cost by Meinel et al. [60]. Additionally, bladder tanks are costed within the same range, as well as a required amount of R245fa which can be stored in contact with N_2 instead of O_2 [61].

A total cost of equipment $\sum PEC_i$ is used to calculate the capital investment cost *CIC*:

$$CIC = \frac{6.32}{OH} \cdot \sum PEC_i \cdot \frac{z(1+z)^n}{(1+z)^n - 1} \quad (33)$$

which refers to the rate of return assuming a fixed interest rate $z = 5\%$, *OH* the operating hours per year, and operation $n = 20$ years. The operation cost *Zi*, is computed with Equation (34) assuming a maintenance operating cost MO = 20% of the total purchase equipment cost $\sum PEC_i$ as:

$$Zi = (MO + CIC) \cdot \frac{PEC_i}{\sum PEC_i} \quad (34)$$

We focus on the total specific cost rate, C_{total} based on the operating cost of each component of the plant *Zi* in $USD, calculated as:

$$C_{total} = \frac{\sum Zi}{\sum P_t - \sum P_p} \quad (35)$$

where total power generated and total power consumption in the pump over the year, $\sum P_t - \sum P_p$ in kWh are considered for normalizing.

3. Results and discussion

3.1. Technical analysis

To test the ORC model described above, concentrating solar radiation is considered as the power source because it has a higher power conversion efficiency compared to flat plate collectors, which are suitable for double-loop systems [62,63]. An average solar radiation is the input of energy that allows the ORC to achieve a condition of 5 K superheated vapor at turbine inlet (see Fig. 1b). Isentropic efficiency is assumed for the pump and the turbine, of 0.7 and 0.8, respectively, while the efficiency of a solar field consisting of parabolic trough collectors (PTC) is calculated using Equation (36) provided by Jaramillo et al. [40]:

$$\eta_{col} = 0.624 - 2.227 \frac{\Delta T_{col}}{q'_{rad}} \quad (36)$$

Any fluid thermodynamic state as well as all the corresponding properties and their magnitude are found in CoolProp wrapper for Python software, which is available in the published literature [53]. The validation of equations of state is based on experimental data for R11, R1233zd(E), R245ca and R245fa, within the established range of pressure and temperature, as found in the published literature [53,64–67]. For this case-study, the solar radiation data shown in Fig. 3 is used, which was registered in Temixco, a small town in Central Mexico, by a solarimetric and meteorological station [68]. This station records the value for global, direct, and diffuse components of solar radiation on a regular basis every 10 min. A full year's averaged data of radiation components shown in Fig. 3 indicates the variation for a daily time between 8:00 and 17:00 h reaching values above 900 W/m^2, which is
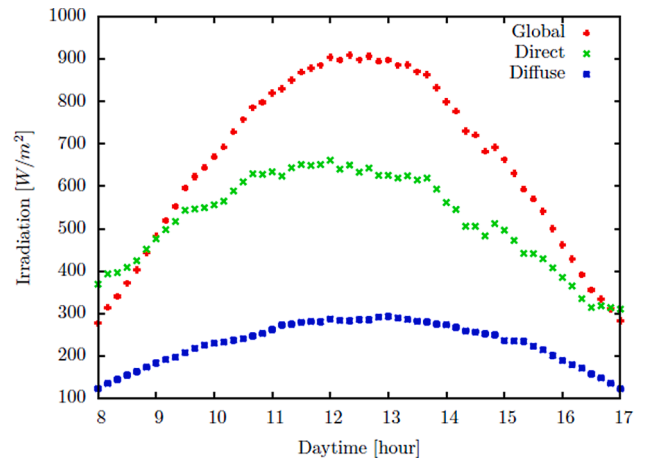

Fig. 3. Registered solar radiation data for one year in Temixco, Morelos, Central Mexico; daily average [68].

considered acceptable for powering the proposed ORC system. Peak values for global radiation between 12:00 and 13:00 h produce a maximum mass flow rate, while the average value of solar energy gives the average value.

3.1.1. ORC performance

The ORC performance is evaluated through the average collector efficiency, the solar radiation incidence surface, the minimum mass flow rate in the turbine and the highest possible thermal efficiency, with basis on the pressure ratio between evaporating and condensing stages in a range $2 \leq P_R \leq 6$, for each one of four selected fluids. The working-fluids thermal stability is warrantied despite any change of mass flow rate in the PTC, required to keep constant the thermodynamic conditions at the turbinés inlet. The purpose of this evaluation is defining the best fluid and pressure ratio for ORC system operation. The range of pressure ratio, rather low, is suitable with a small power output from the PTCs, as well as the designed radial inflow turbine. This is a suitable expander device for the present ORC system [47] and it is recommended in general for small-scale ORC systems [50]. Due to its geometric configuration, which includes variable radius during its operation, radial income turbines are designed for a pressure ratio not higher than 6 [50]; in this case limiting the Mach number at the rotor inlet condition to 0.9 for a rotor velocity not exceeding 27,760 rpm [47]. The efficiency of the solar PTC, where the ORC is in contact with the source of energy, is shown in Fig. 4. The operation starts for a solar radiation incidence on the PTC surface, of low energy and low temperature, according to Fig. 1, which produces a very
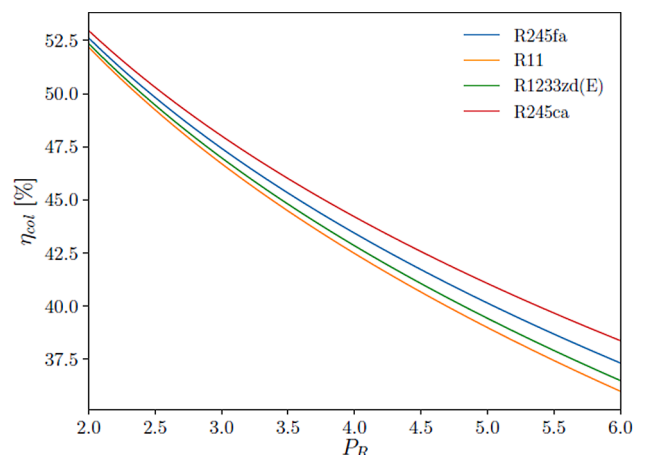

Fig. 4. Average solar collector efficiency as a function of P_R.

small pressure ratio $P_R = 2$ and the higher PTC efficiency, as observed in Fig. 4.

Fig. 4 shows that PTC efficiency, η_{col}, decreases as P_R increases. This is because η_{col} is a function of the temperature difference, see Equation (20), such that the higher ΔT_{col} the lower the efficiency. Fig. 4 indicates also that fluid R245ca produces the best efficiency for the whole range of P_R, while the lowest one is obtained with fluid R11.

The PTC efficiency must agree with incidence surface A_{inc} needed to capture solar energy radiation enough to increase the temperature of the working fluid up to the turbine's inlet thermodynamic conditions. This is shown as a function of P_R in Fig. 5. It is noticed that the surface A_{inc} needed reduces as P_R increases, because a larger pressure ratio P_R demands a higher outlet temperature. It happens like with the mass flow rate in the collector, Fig. 6. This is because the power in the turbine is used as the design parameter: a mass flow rate must ensure such a power which is obtained by means of an iterative process. This mass flow rate is defined by the difference of enthalpy through the turbine, see Equation (8), as higher the P_R higher the turbine inlet enthalpy. Therefore, the mass flow rate reduces as P_R increases, in the same way as the collector surface needed reduces. As observed in Fig. 5, fluid R245ca demands the largest incidence surface for the whole range of P_R. A surface A_{inc} 10% smaller is the best obtained with fluid R11.

The PTC mass flow rate through, $\dot{m}_{col}$, is a key parameter for the ORC system operation, because it varies as well, exposing the turbine to this undesired condition. The results for $\dot{m}_{col}$ are given in Fig. 6, and we observe that $\dot{m}_{col}$ reduces as P_R increases. However, the results show that $\dot{m}_{col}$ is much less sensitive to the fluid. Therefore, this parameter influences little to define best P_R and working fluid for ORC operation.

The ORC system thermal efficiency, η_{th}, is plotted in Fig. 7 against the pressure ratio P_R. As observed, η_{th} grows for any increment of pressure ratio. This is an expected result, given that the efficiency is a function of PTC temperature. As observed in Fig. 7, the performance of the ORC system over the whole range $2 < P_R < 6$ is maximum with fluid R11.

3.1.2. Bladder tanks volume

A contribution of this work to ORC systems is the use of storing working fluid devices, the bladder tanks, to ensure constant fluid flow through the turbine, which must maximize the efficiency. The storing device counteracts the variability of mass flow in the energy collection section. The volume of storage tanks is considered one key factor to obtain as much power in the turbine's shaft as possible, as well as extending its useful life as possible.

Figs. 8 and 9 show the computation of storing volume of pump tank, PST, and turbine tank, TST. Results in Fig. 8 indicates that PST volume reduces as pressure ratio increases. A similar trend is observed for TST volume as observed in Fig. 9. By comparing the volume in these figures,
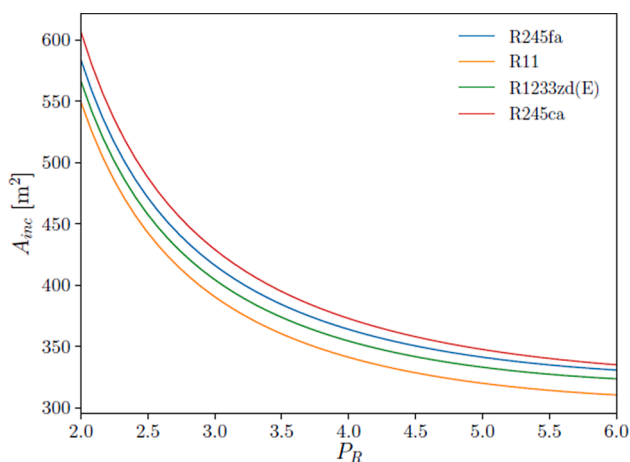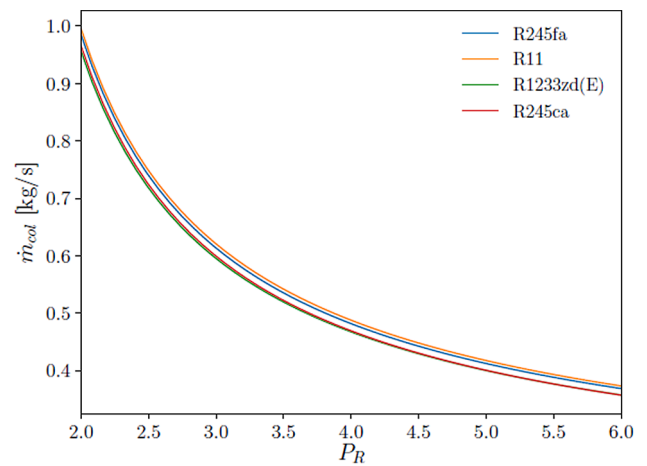

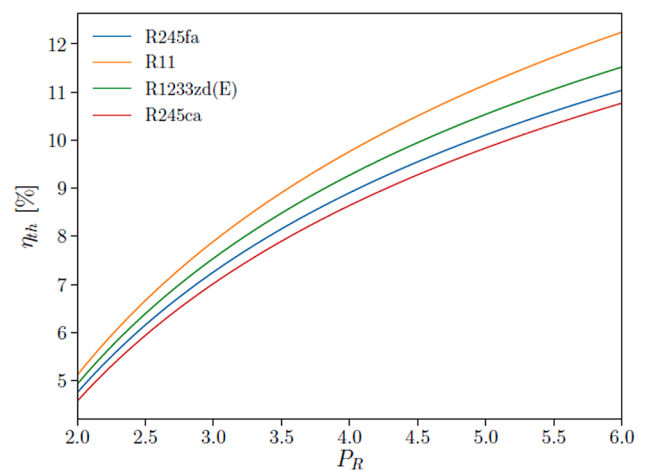**Fig. 6.** Average mass flow rate in the evaporator as a function of P_R.

Fig. 7. Thermal efficiency of ORC system, as a function of the pressure ratio P_R.
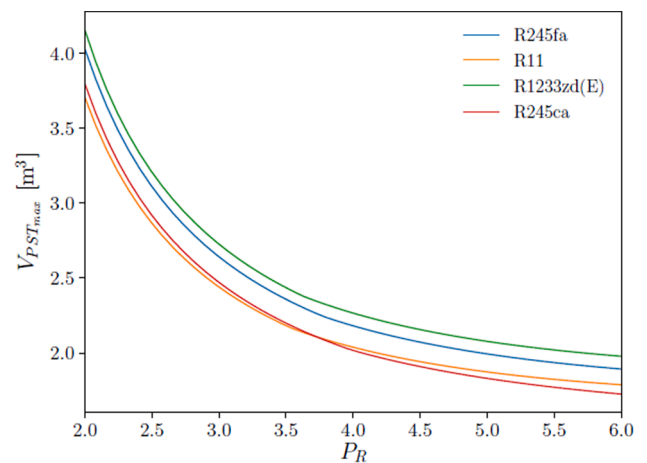

Fig. 8. Volume capacity of PST as a function of P_R.

the PST is considerably smaller than the volume in TST. This is because PST stores saturated liquid, while TST stores superheated vapor. The results indicate that the largest volume of PST is obtained with fluid R1233zd(E) when the ORC system operates at the lowest pressure ratio $P_R = 2$. For this operation condition the PST volume capacity is 4.156 m^3. On the other hand, fluid R245ca leads to an ORC system operating
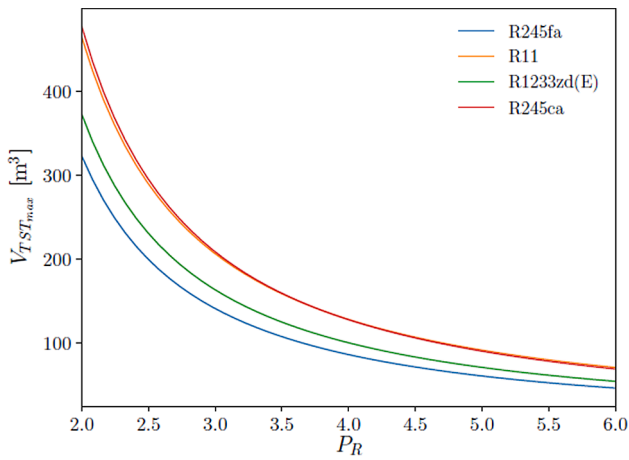

Fig. 5. Solar radiation incidence surface as a function of P_R.

Fig. 9. Volume capacity of TST as a function of P_R.

with the smallest PST volume = 1.726 m^3 for $P_R = 6$.

Based on volume size for TST, Fig. 9, it is much more convenient to operate the ORC system at the highest P_R possible. However, this only occurs during the hours of higher radiation. By using fluid R245ca a tank of 476.678 m^3 is needed for the smaller pressure ratio. This scenario changes if the system operates with fluid R245fa, which requires a TST = 322.586 m^3. Instead, the results with the same fluids for $P_R = 6$ indicate that TST = 71.210 m^3 and 46.705 m^3, respectively. In this respect, R11 shows the largest volume for TST and the smallest volume for the PST. Fluids storing is important for the selection of the working fluid because their impact is reflected on total investment. Small storage tanks are preferred due to space saving, considering the implementation of this ORC system in domestic or commercial applications.

It is worth to remind that a programmed time of 50 min as waiting time for the TST outlet to be opened, is fixed, as required by the operation of the ORC system. However, if P_R increases, the mass flow rate in the solar collector decreases as shown in Fig. 6. This way anomalous operation may occur if the working fluid stored in the TST is not enough for operating the turbine, for certain value of P_R.

To prevent any wrong operation, the fluid in the TST tank is analyzed. From the mass balance in TST, the minimum volume of fluid available in the tank after the waiting time for opening the TST outlet valve is computed as a function of P_R. The results are shown in Fig. 10 where we notice that for a range $4 < P_R < 5$ the fluid stored in the TST, V_{PST}, gets negative values, below 0. This happens for all the working fluids. This anomalous situation indicates that the waiting time is not enough and, therefore, the working fluid in the TST will not be enough
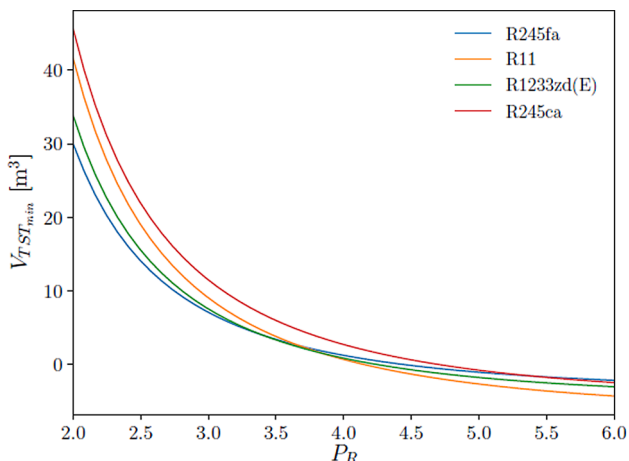
for proper turbine's operation. The solution demands calibration of the computation by increasing a waiting time.

Previous analysis reveals that it is worth operating the ORC system in a range of pressure ratio between 4 and 5. This range is mainly suitable with turbine design, and it is supported by a high thermal efficiency, a low surface of PTC, and lately by a low volume of superheated storage tank, TST. It remains to know what a time-dependence computation throws, with special interest in the dimension of the bladder tanks, which is addressed in the next section.

3.1.3. ORC system performance as a function of time

The ORC system performance as a function of daytime is investigated for suitable pressure ratios $P_R = 4$ and 5. The performance was previously evaluated using a waiting time of 50 min for the TST outlet to be opened, after which the turbine starts its operation. However, an anomalous operation resulted. Therefore, a standby of 60 min is considered, and a comparison of results is conducted. For the analysis, a mass flow rate in the turbine is fixed to 0.5 kg/s. This low flow rate has a purpose to extend the turbine's useful life by reducing as much as possible the rotational speed. A low flow in the turbine also has the advantage of a small outer diameter, which is important given the enthalpy drop that occurs in the expansion [48–51].

The results for PTC efficiency and $P_R = 4$ are plotted against the time in hours in Fig. 11. The trend of η_{col} in this figure reproduces the behavior of the direct component of solar radiation observed in Fig. 1. This is because the design of PTC considers rather direct radiation instead of diffuse. It is observed that collector's performance improves with daytime because the higher radiation of midday produces higher temperatures and thermal energy. Also, the higher PTC performance is obtained with fluid R245ca along the day, and the lesser with fluid R11. A small difference of roughly $\eta_{col} = 3\%$ between the results of R11 and R245ca is observed all along the day, which reduces to minimum values during the sunrise and the sunset hours.

The results for mass flow rate in the evaporator along the day are shown in Fig. 12, where we observe that fluid R11 leads to produce the higher increment of mass flow rate along the midday hours. The influence of the fluid reduces to null difference mass flow rate over both, the sunrise, and the sunset hours. The results in Fig. 12 have the shape of global solar radiation. This happens because there is an influence of the diffuse component on the heat transfer mechanism that defines the magnitude of mass flow rate, as the day advances. However, this influence reduces at midday because of the higher thermal power of direct radiation.

For the ORC system, operating with condition $P_R = 4$, the variations of volume of fluid in the TST and PST along the time are shown in
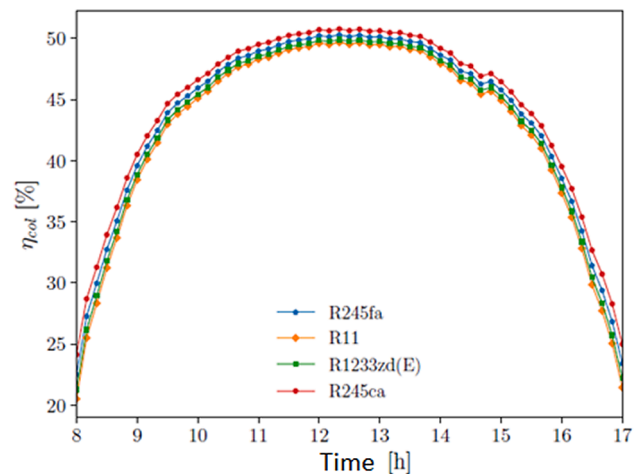

Fig. 10. Minimum fluid volume in TST as a function of P_R.

Fig. 11. Solar collector efficiency along the operating time for the ORC working with $P_R = 4$.
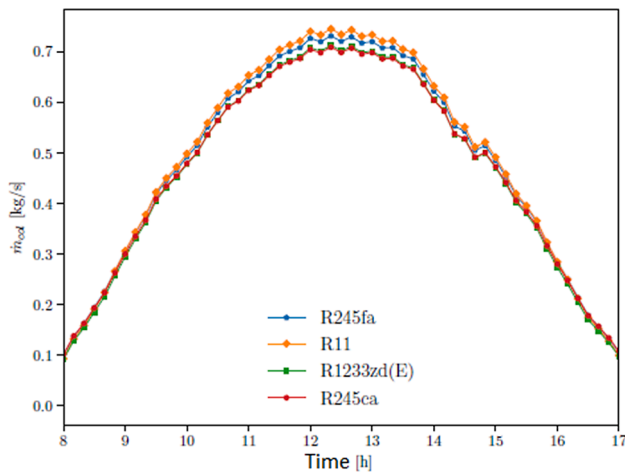
Fig. 12. Mass flow rate in the evaporator along the operating time for the ORC working with $P_R = 4$.

Fig. 14. Volume of working fluid in PST for the ORC working with $P_R = 4$.

Figs. 13 and 14, respectively. As observed, for the volume tanks capacity, it exists a considerable influence of the working fluids. Fig. 13 shows that TST volume increases from very small in the sunrise to maximum in the afternoon, after the hours of higher radiation, then reduces to null at sunset.

A contrary trend characterizes the volume of PST, the tank for saturated liquid. This is because fluid alternates from one tank to another during the daytime. A moderate influence of fluid is observed in the size of PST, as observed in Fig. 14 compared to TST volume size. That influence is higher in PST, where fluids R11 and R245ca are the least demanding of volume, compared against fluids R1233zd(E) and R245fa, being the least demanding the last one. Thermodynamic conditions of working fluid in PST and TST dictated by a density of 1333.4 kg/m³ for saturated liquid in the first compared to 23.809 kg/m³ for superheated vapor in the second produce a fluctuation during the first hours of heating, as observed in Figs. 13 and 14. The first peak in Fig. 13, which occurs close to 9 h in the morning indicates the starting point of the turbine operation leading to starting the generation of electricity that last 8 h.

The calculation showing the fluids variation in the TST along the daytime as a function of the standby time indicates that for $t_e = 50min$ the mass flow in the turbine is assured, is observed in Fig. 15. A standby lesser than 50 min indicates that TST get empty during the first hours of electricity generation.
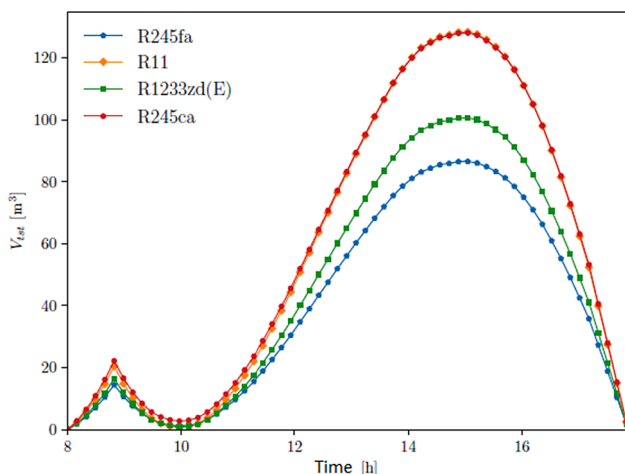
3.1.4. Best operation conditions

The results in previous sections indicate that several parameters must be used to determine the best operation conditions for the ORC system. Table 3 contains the results for $P_R = 4$ and 5. Thermal and collector efficiency are in the first two columns, then we present the results for the mass flow rate in the turbine, followed by the surface of collector PTC, and finally the size of volume required in both tanks, the PST and TST, respectively. For the case $P_R = 4$ it is noticed that the difference in thermal efficiency is 1.12% while the difference between the largest and the smallest TST volume capacity is 41.812 m³, and the difference in the incidence surface for solar radiation is 31.65 m². The mass flow rate for all working fluids is between 0.47 and 0.49 kg/s which satisfies condition $\dot{m}_{turb} = 0.5$ kg/s. The results for TST represent a remainder given that a total investment is influenced by this parameter more than by others.

For a pressure ratio $P_R = 5$ and a standby of 50 min in the TST outflow calculations lead to a negative minimum volume in the PST. To solve this situation, a recalculation considering a standby of 60 min for opening the TST outflow is conducted. The results under these conditions in the same table indicate that higher values are obtained for thermal efficiency, and smaller collectoŕs surface are obtained, except with fluid R245fa. Also, a waiting time slightly higher reduces the volume of TST a 20% for most fluids, except with fluid R1233zd(E). Another advantage of larger waiting time is the mass flow rate in the turbine, which is reduced for all fluids.

The results indicate that fluid R1233zd(E), a standby of 60 min in TST, and a pressure ratio $P_R = 5$ represent the best operating conditions for this ORC system. This statement is based on a series of criteria ordered by importance on performance and cost of equipment. First criterion is due to the mass flow rate, where all fluids give a value close to 0.5 kg/s, with little difference. The volume of TST is a second criterion, where R1233zd(E) also results the second smallest TST volume, 22.5 m³ less than worst R11 volume and its thermal efficiency is the highest, even higher than the one for R11. Third criterion is thermal performance. A 0.61% difference in thermal efficiency is sacrificed for 22.5 m³ in the TST due to the cost of construction and maintenance that could result in this storage tank. Regardless of its thermodynamic performance, R11 is discarded due to it is phase-out because of its high value of ozone depleting potential, ODP. On the other hand, R1233zd(E) is a fourth-generation fluid, thermally stable within the operating conditions, and totally friendly with environment [53–56]. Furthermore, R1233zd(E) is the second best in collector surface, which compensates the cost of a 20% increment compared with R245fa, which seems the second-best option to operate this ORC system after accepting a 0.44% less thermal efficiency.

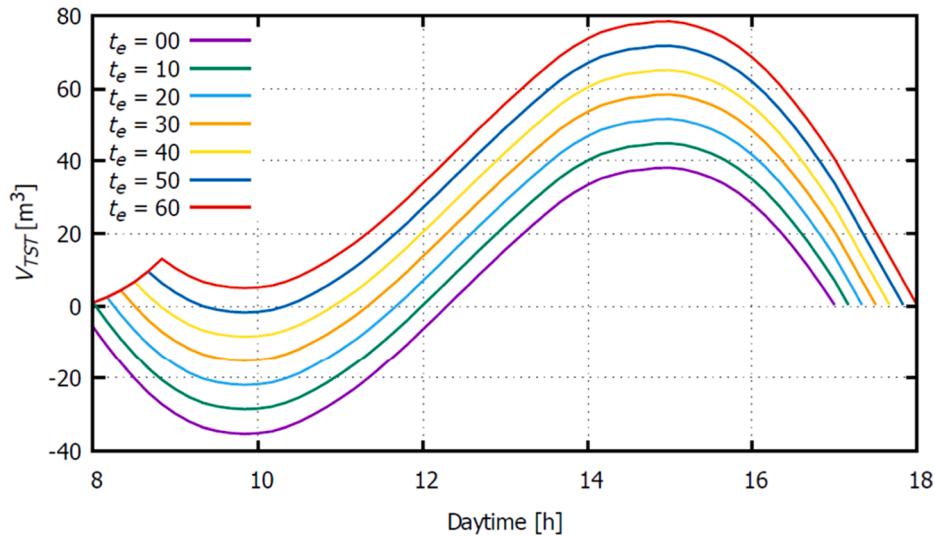In summary, Table 4 presents overall thermodynamic conditions for

Fig. 13. Volume of working fluid in TST for the ORC working with $P_R = 4$.

Fig. 15. Variation of fluid in TST as a function of standby t_e for the R1233zd(E) ORC working and $P_R = 5$.

Table 3

ORC system performance parameters.

Fluid	η_{th} [%]	η_{col} [%]	m_{turb} [kg/s]	A_{inc} [m²]	V_{PST} [m³]	V_{TST} [m³]
$P_R = 4$ and a standby of 50 min						
R245fa	8.91	43.42	0.482	363.79	2.182	86.522
R11	9.76	42.46	0.488	341.03	2.039	128.334
R1233zd(E)	9.27	42.83	0.467	354.27	2.267	100.590
R245ca	8.64	44.19	0.469	372.68	2.019	128.023
$P_R = 5$ and a standby of 60 min						
R245fa	10.11	40.12	0.412	341.11	2.117	66.877
R11	11.15	38.97	0.417	319.84	1.969	100.483
R1233zd(E)	10.54	39.41	0.400	332.94	2.194	78.035
R245ca	9.84	41.05	0.401	347.43	1.962	99.234

Table 4

Thermodynamic conditions in the ORC system (see Fig. 1a) for R1233zd(E) working fluid, $P_R = 5$.

Stage	Pressure (bar)	Temperature (K)	Performance (%)	Equipment
1	1.39	300	100 (isotropic)	condenser, PST
2	6.93	300.37	70	pump
3	6.93	360.32	41.1 average, Eq. (6)	collector
4	1.39	319.85	80 (isentropic)	turbine, TST

all stages 1 to 4, in agreement with Fig. 1a. Columns 2 and 3 show the pressure and temperature corresponding to a mass flow rate of working fluid R1233zd(E), for the condition of maximum solar radiation incidence. The stage equipment and their performance assumed in the computations are include in column 4. Storage bladder tanks PST and TST are assumed isentropic. The design of bladder tanks, which involves the selection of one elastomer with material properties according to thermodynamic conditions for stages 1 and 4 is not addressed because it is out of the scope of this paper.

3.2. ORC economic performance

As in any electricity generation system, the price of equipment in an

ORC varies as a function of the output, being more expensive as smaller the scale. A list of small-scale turbines from different makers is given in Table 5 [69]. Although the cost per kW in this table is competitive, the installation requires more consideration; for instance, a power block, which includes the generator and connection system to the grid besides the turbine. It varies from 830 to 1190 $/kWe, for a solar energy plant larger than 9 MW [70,71]. Therefore, the actual cost may be higher for the plant than discussed in this work given the change of prices as a function of time, local expansion of clean sources policies, and the evolution of renewable power market. The energy source has no cost, but the PT-collector represents a wealth of the plant equipment cost. Their price depends on cost fluctuations of main materials like aluminum, at rates between 170 and 270 $/m2 for a high technology system recently developed by the National Renewable Research Laboratory [72,73]. An estimate per kW of plant costs and investment for the economics analysis is given in Table 6 following Equation (32)–(35) and the data from Table 2 discussed in Section 2.5 above.

Since column 2 of Table 6 represents an indicator of the cost of the ORC system, in real installations it depends on prices and taxes applicable for each case. The operation cost Z_i given in column 3, represents the yearly amount needed for keeping all elements working as scheduled. A specific cost C_i is obtained from the last column. It represents the costs in cents of dollar per kWh of generated electricity. As a result, a total cost, 8 h operating time each day of the year, $C_{total}= 0.0543$ $/kWh is obtained, which is better than the value for an ORC plant of output 0.5 MW reported by Meinel et al. [60].

For comparison of present results, we present data of global cost of electricity generation for different technologies as shown in Table 7. Data from the International Renewable Energy Agency (IREA) correspond to 2019 [72], while this year's report from the US Energy Information Administration (US-EIA) was consulted [73]. The solar photovoltaic option seems competitive against other technologies. However, an ORC system may be scalable to cover small and medium

Table 5

Costs of turbines for ORC system [69].

Supplier	Model	Speed (rpm)	Output (kW)	Unit cost ($/kW)
Solar	(TAURUS)	14,950	4.370	434.78
Nuovo Pignone	(PGT10)	7900	9.980	521.04
Solar	(MARS)	9000	10	460.00
Mitsubishi	(MF11A)	9660	12.835	451.89
GE	(LM1600)	7000	13.430	513.78
RR	(AVON)	5500	14.6	328.54

Table 6
Costs for ORC system.

i equipment	$PEC_{i_{sp}}$ ($/kW)	Zi_{sp} ($/kW)	C_i ($/kWh)
1 pump	3000	33.07	0.001265
2 condenser	26,000	286.57	0.010965
3 turbine	20,000	220.44	0.001327
4 PTC	60,700	669.22	0.025607
5 TST	11,000	121.24	0.004639
6 PST	8000	88.18	0.003374

Table 7
Current competitive price of electricity upon the technology.

Generating technology	IREA $/MWh	US-EIA $/MWh	Present design $/MWh
Concentrating Solar power	182		54.3
Wind onshore	53	39.95	
Solar PV	68	35.74	

demand such that the specific application is decisive. Further, although reduced in power capacity another possible option for replacing the concentrating energy are flat-plate solar collectors which are cheaper, provided the required temperature of 35–40 °C above ambient is achieved [74].

Advantage of subsidiary programs in several countries where the utility cost of electricity is lower than the price paid to private producers can apply. Specially if the electricity that goes into the grid comes from renewable sources like solar. The incentives may be interesting because of the policy for the development of green energy. Electricity delivered to the grid at a regular price $ 0.045/kWh in a medium-size country is possible [75]. A revenue is calculated under this scheme such that for the six months of the year with the highest temperature, the first 300 kWh cost 20.76% of the regular price, the next 900 kWh consumed cost 25.93% of the regular price, and then the next 1300 kWh consumed cost 63.10% of the regular price. In the rest of the year, the subsidy is as follows: the first 75 kWh consumed cost 28.29% of the regular price, the next 125 kWh consumed cost 34.12% of the regular price. Under this scenario the revenue is expected at $2904.56/year compared to the operation and maintenance cost $1418.71/year, calculated from Equation (34), reducing the time for return of capital investment. It makes the electricity generation with the ORC analyzed a technically and economically feasible renewable energy application.

4. Conclusions

A novel solar assisted ORC system of single working fluid was modeled and simulated. The system considers a bladder tank between the trough collector and the turbine that ensures a constant mass flow rate in the turbine despite the natural variation of solar energy input. Thus, the reliability of the system increases, and the total cost is reduced during the operation by extending the useful life of turbine as possible. The results show an enhanced thermal efficiency of 10.54% for the ORC system that generates 10 kW during 8 h/day at averaged total cost of 54.3 $/MWh using R1233zd(E), and a pressure ratio $P_R = 5$ powered by averaged solar radiation of 900 W/m^2. The study of specific investment cost shows a high level of competitiveness highlighting the advantages of a single-fluid single-loop ORC system design through reduced heat transfer losses compared with reported data of larger scale power generation systems.

Future work. It is envisaged that the results in the paper be complemented with a parametric study with the purpose of identifying the main constraints in scaling the ORC, given that the potential of application can increase. It is also envisaged that the bladder tanks need to be carefully designed based on the material properties of the internal membrane. These properties must be selected to obtain the longest

useful life under daily elongation-contraction in conditions of the stages 1 and 4 of the ORC.

CRediT authorship contribution statement

U. Caldiño Herrera: Conceptualization, Investigation, Formal analysis, Data curation. **J.C. García:** Methodology, Supervision, Writing - original draft. **F.Z. Sierra-Espinosa:** Conceptualization, Methodology, Supervision, Writing - review & editing, Data curation. **J.A. Rodríguez:** Investigation. **O.A. Jaramillo:** Investigation. **O. De Santiago:** Investigation. **S. Tilvaldiev:** Visualization.

Declaration of Competing Interest

The authors declare that they have no known competing financial interests or personal relationships that could have appeared to influence the work reported in this paper.

References

[1] E.A. Alp, Energy consumption and economic growth in OECD countries, Int. J. Energy Econ. Policy 6 (2016) 753–759.
[2] M. Villarini, E. Bocci, M. Moneti, A. Di Carlo, A. Micangeli, State of art of small scale solar powered ORC systems: A review of the different typologies and technology perspectives, Energy Procedia 45 (2014) 257–267.
[3] J.B. Obi, State of art on ORC applications for waste heat recovery and micro-cogeneration for installations up to 100 kWe, Energy Procedia 82 (2015) 994–1001.
[4] W. Pu, C. Yue, D. Han, W. He, X. Liu, Q. Zhang, Y. Chen, Experimental study on Organic Rankine cycle for low grade thermal energy recovery, Appl. Therm. Eng. 94 (2016) 221–227.
[5] V. Maizza, A. Maizza, Unconventional working fluids in organic Rankine-cycles for waste energy recovery systems, Appl. Therm. Eng. 21 (2001) 381–390.
[6] K. Rahbar, S. Mahmoud, R.K. Al-Dadah, N. Moazami, S.A. Mirhadizadeh, Review of organic Rankine cycle for small-scale applications, Energy Convers. Manage. 134 (2017) 135–155.
[7] D. Ziviani, A. Beyene, M. Venturini, Advances and challenges in ORC systems modeling for low grade thermal energy recovery, Appl. Energy 121 (2014) 79–95.
[8] S. Quoilin, M. Van Den Broek, S. Declaye, P. Dewallef, V. Lemort, Techno-economic survey of Organic Rankine Cycle (ORC) systems, Renew. Sustain. Energy Rev. 22 (2013) 168–186.
[9] A. Schuster, S. Karellas, E. Kakaras, H. Spliethoff, Energetic and economic investigation of Organic Rankine Cycle applications, Appl. Therm. Eng. 29 (2009) 1809–1817.
[10] L. Da Lio, G. Manente, A. Lazzaretto, A mean-line model to predict the design efficiency of radial inflow turbines in organic Rankine cycle (ORC) systems, Appl. Energy 205 (2017) 187–209.
[11] R. L. Fuller, Conversion of low temperature waste heat utilizing hermetic organic Rankine cycle. Final Report: DE 2006838860, 2005.
[12] https://orc-world-map.org/. World Overview of the Organic Rankine Cycle technology (accessed: 445 2019-04-11).
[13] B. Dong, G. Xu, X. Luo, L. Zhuang, Y. Quan, Potential of low temperature organic Rankine cycle with zeotropic mixtures as working fluid, Energy Procedia 105 (2017) 1489–1494.
[14] D. Tillmanns, C. Gertig, J.S. Gibelhaus, U. Bau, F. Lanzerath, A. Bardow, Integrated design of ORC process and working fluid using PC-SAFT and Modelica, Energy Procedia 139 (2017) 97–104.
[15] T. Hung, S. Wang, C. Kuo, B. Pei, K. Tsai, A study of organic working fluids on system efficiency of an ORC using low-grade energy sources, Energy 35 (2010) 1403–1411.
[16] A.I. Papadopoulos, M. Stijepovic, P. Linke, On the systematic design and selection of optimal working fluids for Organic Rankine Cycles, Appl. Therm. Eng. 6–7 (2010) 760–769.
[17] X.D. Wang, L. Zhao, J.L. Wang, W.Z. Zhang, X.Z. Zhao, W. Wu, Performance evaluation of a low-temperature solar Rankine cycle system utilizing R245fa, Sol. Energy 84 (2010) 353–364.
[18] J.L. Wang, L. Zhao, X.D. Wang, An experimental study on the recuperative low temperature solar Rankine cycle using R245fa, Appl. Energy 94 (2012) 34–40.
[19] M. Wang, J. Wang, Y. Zhao, P. Zhao, Y. Dai, Thermodynamic analysis and optimization of a solar-driven regenerative organic Rankine cycle (ORC) based on flat-plate solar collectors, Appl. Therm. Eng. 50 (2013) 816–825.

[20] J. Zhang, L. Zhao, J. Wen, S. Deng, An overview of 200 kW solar power plant based on organic Rankine cycle, Energy Procedia 88 (2016) 356–362.

[21] A.M. Delgado-Torres, L. García-Rodríguez, Analysis and optimization of the low-temperature solar organic Rankine cycle (ORC), Energy Convers. Manage. 51 (2010) 2846–2856.

[22] A.M. Delgado-Torres, L. García-Rodríguez, Design recommendations for solar organic Rankine cycle (ORC) powered reverse osmosis (RO) desalination, Renew. Sustain. Energy Rev. 16 (2012) 44–53.

[23] F. Calise, M.D. D'Accadia, M. Vicidomini, M. Scarpellino, Design and simulation of a prototype of a small-scale solar CHP system based on evacuated flat-plate solar collectors and Organic Rankine Cycle, Energy Convers. Manage. 90 (2015) 347–363.

[24] J. Freeman, I. Guarracino, S.K. Markides, A small-scale solar organic Rankine cycle combined heat and power system with integrated thermal energy storage, Appl. Therm. Eng. 127 (2017) 1543–1554.

[25] J. Freeman, K. Hellgardt, C.N. Markides, An assessment of solar-powered organic Rankine cycle systems for combined heating and power in UK domestic applications, Appl. Energy 138 (2015) 605–620.

[26] J. Freeman, K. Hellgardt, C.N. Markides, Working fluid selection and electrical performance optimization of a domestic solar-ORC combined heat and power system for year-round operation in the UK, Appl. Energy 186 (2017) 291–303.

[27] S. Quoilin, M. Orosz, H. Hemond, V. Lemort, Performance and design optimization of a low-cost solar organic Rankine cycle for remote power generation, Sol. Energy 85 (2011) 955–966.

[28] A. Abhat, Low temperature latent heat thermal energy storage: heat storage materials, Sol. Energy 30–4 (1983) 313–332.

[29] B. Zalba, J.M. Marin, L.F. Cabeza, H. Mehling, Review on thermal energy storage with phase change: materials heat transfer analysis and applications, Appl. Therm. Eng. 23 (2003) 251–283.

[30] F. Agyenim, N. Hewitt, P. Eames, M. Smyth, A review of materials, heat transfer and phase change problem formulation for latent heat thermal energy storage systems (LHTESS), Renew. Sustain. Energy Rev. 14 (2010) 615–628.

[31] M. Liu, W. Saman, F. Bruno, Review on storage materials and thermal performance enhancement techniques for high temperature phase change storage system, Renew. Sustain. Energy Rev. 16 (2012) 2118–2132.

[32] E. Oro, A. de Garcia, A. Castell, M.M. Farid, L.F. Cabeza, Review on phase change materials for cold thermal energy storage applications, Appl. Energy 99 (2012) 513–533.

[33] Y. Lin, Y. Jia, G. Alva, G. Fang, Review on thermal conductivity enhancement, thermal properties and applications of phase change materials in thermal energy storage, Renew. Sustain. Energy Rev. 82 (2018) 2730–2742.

[34] A. Groniewsky, G. Györke, A. Imre, Description of wet-to-dry transition in model ORC working fluids, Appl. Therm. Eng. 125 (2017) 963–971.

[35] S. Rani*, A.K. Agrawal, V. Rastogi, Vibration analysis for detecting failure mode and crack location in first stage gas turbine blade, J. Mech. Sci. Technol. 33 (I) (2019) 1–10.

[36] O.S. Salawu, Detection of structural damage through changes in frequency: A review, Eng. Struct. 19 (1997) 718–723.

[37] J.C. García, F.Z. Sierra*, Vibration failure in admission pipe of a steam turbine due to flow instability, Eng. Failure Anal. 27 (2013) 30–40.

[38] W.B. Young, Advantages of bladder surge tanks in pipelines, in: Paper PVP 2012-78613 ASME 2012 Pressure Vessels and Piping Conf., vol. 3, 2012, pp. 687–692.

[39] A. Ravve, Principles of Polymer Chemistry, third ed., Springer, NY, 2012.

[40] O.A. Jaramillo, M. Borunda, K. Velazquez-Lucho, M. Robles, Parabolic trough solar collector for low enthalpy processes: An analysis of the efficiency enhancement by using twisted tape inserts, Renew. Energy 93 (2016) 125–141.

[41] J. Bao, L. Zhao, A review of working fluid and expander selections for organic Rankine cycle, Renew. Sustain. Energy Rev. 24 (2013).

[42] O.E. Bajle, Turbomachines, A Guide to Design, Selection and Theory, Wiley, 1981. ISBN 9780471060369.

[43] O.E. Bajle, A study on design criteria and matching turbomachinery: Part a-similarity relations and design criteria of turbines, J. Eng. Power 84–1 (1962) 83–102, https://doi.org/10.1115/1.3673386.

[44] A. Meroni, M. Robertson, R. Martinez-Botas, F. Haglind, A methodology for the preliminary design and performance prediction of high-pressure ratio radial-inflow turbines, Energy 164 (2018) 1062–1078.

[45] Yan Li, Xiao-dong Ren, Investigation of the organic Rankine cycle (ORC) system and the radial-inflow turbine design, Appl. Therm. Eng. 96 (2016) 547–554.

[46] M. Deligant, E. Sauret, Q. Danel, F. Bakir, Performance assessment of standard radial turbine as turbo expander for an adapted solar concentration ORC, Renew. Energy 147–3 (2020) 2833–2841, https://doi.org/10.1016/j.renene.2018.10.019.

[47] U. Caldiño Herrera, J. C. García, F.Z. Sierra-Espinosa, JO. D'avalos, M.A. Lira, Radial inflow turbine geometry generation method using third order Bezier curves for blade design, Paper: GT2019-90163, Proc. ASME Turbo Expo 2019, June 11-15, 2019, Phoenix, USA.

[48] H. Moustapha, M.F. Zelesky, N.C. Baines, D. Japikse, Axial and Radial Turbines, first ed., Concepts NREC, 2003.

[49] S.L. Dixon, C.A. Hall, Fluid Mechanics and Thermodynamics of Turbomachinery, sixth ed., Butterworth-Heinemann, 2010.

[50] E.A. Baskharone, Principles of Turbomachinery in Air-Breathing Engines, first ed., Cambridge University Press, 2006.

[51] H.A. Ronald, Turbine Aerodynamics, first ed., ASME Press, 2005.

[52] P.F. Boulos, B.W. Karney, D.J. Wood, S. Lingireddy, Hydraulic Transient Guidelines for Protecting Water Distribution Systems, Am. Water Works Assoc. 97 (2005).

[53] I.H. Bell, J. Wronski, S. Quoilin, V. Lemort, Pure and pseudo-pure fluid thermophysical property evaluation and the open-source thermophysical property library CoolProp, Ind. Eng. Chem. Res. 53 (2014) 2498–2508.

[54] H. M. Curran, Use of organic working fluids in Rankine engines, Report No. DOE/CS/30202-T1, Hittman Assoc. Inc., Columbia, MD, 1979.

[55] C. Mateu-Royo, J. Navarro-Esbrí, A. Mota-Babiloni, M. Amat-Albuixech, F. Molés, Thermodynamic analysis of low GWP alternatives to HFC-245fa in high-temperature heat pumps: HCFO-1224yd (Z), HCFO-1233zd (E) and HFO-1336mzz (Z), Appl. Therm. Eng. 152 (2019) 762–777.

[56] https://msds-resource.honeywell.com/ehswww/hon/result/result_single.jsp?P_LANGU=E&P_SYS=1&C001=MSDS&C997=C100%3BESDS_US%2BC102%3BUS%2B1000&C100=*&C101=*&C102=*&C005=000000009878&C008=&C006=HON&C013.

[57] R. Jacobsen, S. Penoncello, E. Lemmon, A fundamental equation for trichlorofluoromethane (R-11), Fluid Phase Equilib. 80 (1992) 45–56.

[58] R. Turton, R.C. Bailie, W.B. Whiting, J.A. Shaeiwitz, Analysis, Synthesis and Design of Chemical Processes, third ed., Prentice Hall, 2009.

[59] F. Heberle, P. Bassermann, M. Preißinger, D. Brüggemann, Exergoeconomic optimization of an organic Rankine cycle for low-temperature geothermal heat sources, Int. J. Thermodyn. 15 (2) (2012) 119–126.

[60] D. Meinel, Ch. Wieland, H. Spliethoff, Economic comparison of ORC (Organic Rankine cycle) processes at different scales, Energy 74 (2014) 694–706.

[61] http://www.honeywell-genetron-245fa-orc-systems-brochure1.

[62] B. Twomey, P.A. Jacobs, H. Gurgenci, Dynamic performance estimation of small-scale solar cogeneration with an organic Rankine cycle using a scroll expander, Appl. Therm. Eng. 51 (2013) 1307–1316.

[63] K.H. Kim, C.H. Han, A review on solar collector and solar organic Rankine cycle (ORC) systems, J. Autom. Control Eng. 3–1 (2015) 66–73.

[64] Y. Zhou, E.W. Lemmon, Equation of State for the Thermodynamic Properties of 1,1,2,2,3-Pentafluoropropane (R-245ca), Int. J. Thermophys. 37 (2016) 27.

[65] M.E. Mondéjar, M.O. McLinden, E.W. Lemmon, Thermodynamic Properties of trans-1-Chloro-3,3,3-trifluoropropene (R1233zd(E)): Vapor Pressure, (p, r, T) behavior, and speed of sound measurements, and equation of state, J. Chem. Eng. Data 60–8 (2015) 2477–2489.

[66] R. Akasaka, A fundamental equation of state for 1,1,1,3,3-pentafluoropropane (R-245fa), J. Phys. Chem. Ref. Data 44 (013104) (2015) 2477–2489.

[67] G. Györke, U.K. Deiters, A. Groniewsky, I. Lassu, R. Imre, A Novel classification of pure working fluids for Organic Rankine Cycle, Energy 145 (2018) 288–300.

[68] Renewable Energy Institute, National Autonomous University of Mexico, UNAM, Consults ESOLMET-IER, 2017.

[69] Nye Thermodynamics Corp., http://www.nyethermodynamics.com/kwprices, 2019.

[70] C. Turchi, M. Mehos, C.K. Ho, G.J. Kolb, Current and future costs for parabolic trough and power systems in the US market, in: Proc. SolarPACES, Perpignan, Fr., September 21-24, 2010.

[71] P. Kurup and C. S. Turchi, Parabolic Trough Collector Cost Update for the System Advisor Model (SAM), National Renewable Energy Laboratory, Technical Report NREL/TP-6A20-65228, 2015.

[72] https://www.irena.org/publications/2020/Jun/Renewable-Power-Costs-in-2019.

[73] https://www.eia.gov/outlooks/aeo/pdf/AEO2020%20Full%20Report.pdf.

[74] S. Farahat, F. Sarhaddi, H. Ajam, Exergetic optimization of flat plate solar collectors, Renewable Energy 34 (2009) 1169–1174.

[75] https://app.cfe.mx/Aplicaciones/CCFE/Tarifas/TarifasCRECasa/Tarifas/Tarifa1.aspx.